

# HENRY

Hydraulic Engineering Repository

Ein Service der Bundesanstalt für Wasserbau

---

Conference Paper, Published Version

**Alves, E.; Ferreira, Rui; Cardoso, A. H.**

## **One-dimensional numerical modelling of turbidity currents: hydrodynamics and deposition**

---

Verfügbar unter/Available at: <https://hdl.handle.net/20.500.11970/99756>

Vorgeschlagene Zitierweise/Suggested citation:

Alves, E.; Ferreira, Rui; Cardoso, A. H. (2010): One-dimensional numerical modelling of turbidity currents: hydrodynamics and deposition. In: Dittrich, Andreas; Koll, Katinka; Aberle, Jochen; Geisenhainer, Peter (Hg.): River Flow 2010. Karlsruhe: Bundesanstalt für Wasserbau. S. 1097-1104.

### **Standardnutzungsbedingungen/Terms of Use:**

Die Dokumente in HENRY stehen unter der Creative Commons Lizenz CC BY 4.0, sofern keine abweichenden Nutzungsbedingungen getroffen wurden. Damit ist sowohl die kommerzielle Nutzung als auch das Teilen, die Weiterbearbeitung und Speicherung erlaubt. Das Verwenden und das Bearbeiten stehen unter der Bedingung der Namensnennung. Im Einzelfall kann eine restriktivere Lizenz gelten; dann gelten abweichend von den obigen Nutzungsbedingungen die in der dort genannten Lizenz gewährten Nutzungsrechte.

Documents in HENRY are made available under the Creative Commons License CC BY 4.0, if no other license is applicable. Under CC BY 4.0 commercial use and sharing, remixing, transforming, and building upon the material of the work is permitted. In some cases a different, more restrictive license may apply; if applicable the terms of the restrictive license will be binding.



# One-dimensional numerical modelling of turbidity currents: hydrodynamics and deposition

Elsa Alves

*Hydraulics and Environment Department, Laboratório Nacional de Engenharia Civil (LNEC); Av. Brasil, 101, 1700-066 Lisboa, Portugal*

Rui M. L. Ferreira & António H. Cardoso

*CEHIDRO – Instituto Superior Técnico, TULisbon; Av. Rovisco Pais, 1049-001 Lisboa, Portugal*

**ABSTRACT:** Turbidity currents may play an important role on reservoir sedimentation as they are capable of transporting large quantities of fine sediments over long distances towards the dam. In this paper, a one-dimensional numerical model for the simulation of turbidity currents driven by non-cohesionless uniform sediment is presented. The layer-averaged governing equations are solved numerically using a second-order total variation diminishing method of the Godunov-type. The HLLC approximate Riemann solver is used for the computation of numerical fluxes. The performance of the numerical model is verified against laboratory experiments performed for this study and with laboratory data from other authors. Close agreement is achieved in reproducing the mean current features and deposits.

*Keywords:* Turbidity currents; Numerical models; HLLC approximate Riemann solver; WAF

## 1 INTRODUCTION

In many reservoirs, the transport and deposition of fine sediments are associated with turbidity currents events. These currents are generated when the sediment-laden river inflow enters a reservoir and plunges below the clear quiescent water and continues as a dense underflow. Driven by the density difference caused by suspended fine sediments, turbidity currents are capable of transport large amounts of sediments over long distances and eventually reach the dam.

Prediction of the evolution of turbidity currents is of great interest to many reservoir engineering problems. Sediment deposition by turbidity currents will contribute to reservoir loss of water storage capacity, obstruction of the bottom outlets, or interfere with the operation of the intake structures and affect the reservoir ecology. In reservoirs where turbidity currents are frequent events, the control of sedimentation can be done by venting these currents through the opening of the low-level outlets at the dam (Fan & Morris 1992, ICOLD 1999) or by controlling the phenomena using obstacles placed in the reservoirs (Oehy & Schleiss 2007). For the success of these measures, turbidity currents characteristics must be known or predicted using adequate numerical models.

Over the last decades, continuing effort has been made to develop numerical models for unsteady turbidity currents simulation. Most of these models are based on one and two-dimensional (1D and 2D) depth-averaged single layer formulations (1D: Choi & García 1995, Sloff 1997, Kostic & Parker 2003, Kostic & Parker 2006; 2D: Choi 1998, Bradford & Katopodes 1999). The depth-averaged formulation consists of a hyperbolic system of partial differential equations derived by Parker et al. (1986) by averaging the vertical structure of the flow over the depth.

An important concern for numerical methods when solving hyperbolic equations is the ability to deal with discontinuities in the flow variables. In particular, to simulate turbidity currents the model must be able not only to predict the flow hydrodynamics, erosion and deposition but also to deal with the propagation of a front and the possible occurrence of internal hydraulic jumps.

Godunov-type schemes are especially suitable for capturing discontinuities in the flow. Several researchers have applied successfully the HLL (Harten, Lax and van Leer) approximated Riemann Solver for the Euler equations (Toro et al. 1994) and for the shallow water equations (Fraccarollo & Toro 1995, Fraccarollo et al. 2003, Cao et al. 2004). The robustness and simplicity of this

solver provided the motivation for its application to the simulation of turbidity currents.

In this paper, the HLLC Riemann solver proposed by Toro et al. (1994) has been implemented in a second-order total variation diminishing method. The numerical model results were verified using available laboratory data.

This paper is organized as follows: In section 2 the governing equations of the flow are presented and in section 3 the proposed numerical scheme is described. In section 4 the computational scheme is applied to the simulation of turbidity currents and the results are compared with laboratory data. Finally, conclusions are drawn in section 5.

## 2 GOVERNING EQUATIONS

The spatial development of an unsteady, one-dimensional, turbidity current flowing in deep ambient fluid (Fig. 1) can be described by the following set of layer-averaged partial differential equations derived by Parker et al. (1986):

$$\frac{\partial h}{\partial t} + \frac{\partial Uh}{\partial x} = E_w U \quad (1)$$

$$\frac{\partial Uh}{\partial t} + \frac{\partial U^2 h}{\partial x} = -\frac{1}{2} Rg \frac{\partial Ch^2}{\partial x} + RCghS - u_*^2 \quad (2)$$

$$\frac{\partial Ch}{\partial t} + \frac{\partial CUh}{\partial x} = w_s (E_s - c_b) \quad (3)$$

where  $h$  = current thickness,  $U$  = layer-averaged velocity,  $C$  = layer-averaged suspended sediment concentration,  $R = (\rho_s - \rho)/\rho$ , where  $\rho_s$  = sediment density and  $\rho$  = density of the ambient fluid,  $S$  = bottom slope,  $g$  = acceleration due to gravity,  $u_*$  = shear velocity,  $E_w$  = ambient fluid entrainment coefficient,  $E_s$  = sediment entrainment coefficient,  $w_s$  = particle fall velocity, and  $c_b$  = near-bed sediment concentration.

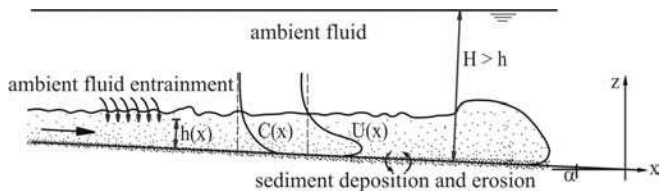


Figure 1. Definition sketch

Equations (1) and (3) are the fluid and sediment mass continuity equations and Equation (2) the momentum equation. In the continuity equation the term  $E_w U$  represents the rate of ambient fluid entrainment into the current. The term  $w_s (E_s - c_b)$  is the net entrainment flux from the bed to the current due to erosion and deposition. The dependent variables are  $h$ ,  $U$  and  $C$ .

The bed-sediment conservation equation is

$$(1 - \lambda) \frac{\partial z}{\partial t} = w_s (c_b - E_s) \quad (4)$$

where  $z$  = bed elevation and  $\lambda$  = porosity of the bed.

In order to solve the governing equations given above, closure relationships for the fluid and sediment entrainment coefficients, shear velocity and concentration near the bed must be specified. Based on experimental data, Parker et al. (1987) obtained the following expression for the ambient fluid entrainment coefficient:

$$E_w = \frac{0.075}{(1 + 718 Ri)^{0.5}} \quad (5)$$

where  $Ri = gRhC/U^2$  is the bulk Richardson number. The sediment entrainment coefficient is determined from the empirical relationship proposed by Parker et al. (1987):

$$E_s = \frac{3 \times 10^{-11} \zeta^7}{1 + 10^{-10} \zeta^7} \quad (6)$$

where  $\zeta$  is defined by

$$\zeta = \frac{u_*}{w_s} Re_p^{0.75} \quad (7)$$

and  $Re_p$  denotes the particle Reynolds number ( $Re_p = (gRD^3)^{0.5}/\nu$  where  $D$  = particle diameter).

In the experiments conducted by Parker et al. (1987), a simple relation between near-bed and layer-averaged concentrations was found:

$$\frac{c_b}{C} \cong 2 \quad (8)$$

The relation for shear velocity is

$$u_*^2 = C_D U^2 \quad (9)$$

where  $C_D$  is a coefficient of bed friction. A typical range of  $C_D$  values is 0.002-0.1 including experimental and field data (Parker et al. 1987).

## 3 NUMERICAL MODEL

The governing equations are of hyperbolic type (Bradford et al. 1997), admitting shocks and discontinuities. The one-dimensional equations in the conservative form can be written as:

$$\frac{\partial \mathbf{U}}{\partial t} + \frac{\partial \mathbf{F}}{\partial x} = \mathbf{Q} \quad (10)$$

where  $\mathbf{U}$  = vector of conservative variables,  $\mathbf{F}$  = flux vector and  $\mathbf{Q}$  = source term vector given by

$$\mathbf{U} = \begin{bmatrix} h \\ hU \\ hC \end{bmatrix}, \quad \mathbf{F} = \begin{bmatrix} hU \\ hU^2 + \frac{1}{2}gRh^2C \\ hUC \end{bmatrix} \quad (11a,b)$$

$$\mathbf{Q} = \begin{bmatrix} E_w U \\ -gRhC \frac{\partial z}{\partial x} - u_*^2 \\ w_s (E_s - c_b) \end{bmatrix} \quad (11c)$$

A cell-centered finite volume method is formulated for Eq. (10). The computational domain  $[0,L]$  is divided into  $N$  cells and the points  $x_i$  are the centres of the cells. An explicit conservative discretization form of Eq. (10) can be written as

$$\mathbf{U}_i^{n+1} = \mathbf{U}_i^n - \frac{\Delta t}{\Delta x} (\mathbf{F}_{i+1/2}^n - \mathbf{F}_{i-1/2}^n) + \Delta t \mathbf{Q}_i^n \quad (12)$$

where  $\mathbf{U}_i^n$  = average of  $\mathbf{U}$  in cell  $i$  at time level  $n$ ,  $\Delta x$  = width of the cell  $i$ ,  $\Delta t$  = time step,  $\mathbf{F}_{i+1/2}^n$ ,  $\mathbf{F}_{i-1/2}^n$  = fluxes at cell interfaces and  $\mathbf{Q}_i^n$  = average of  $\mathbf{Q}$  in cell  $i$ .

In Godunov-type schemes the numerical flux  $\mathbf{F}_{i+1/2}^n$  is computed from the exact or approximate solution of a Riemann problem at the interface  $i+1/2$ .

In the present model, the HLLC (Harten, Lax and van Leer and Contact surface) approximate Riemann solver (Toro et al. 1994 and Toro 1999) is adopted to calculate the flux vector at each cell interface. This solver assumes a simplified wave configuration for the solution of the Riemann problem consisting of three waves of speed  $S_L$ ,  $S_R$  and  $S^*$  separating four constant states (see Fig. 2).

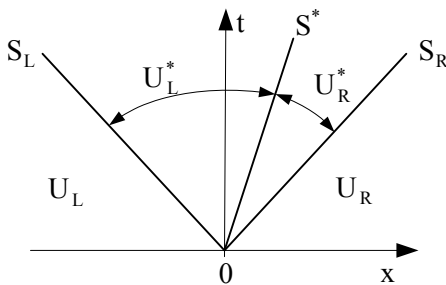


Figure 2. Wave structure for the HLLC Riemann solver

The HLLC Riemann solver is given by

$$\mathbf{F}_{i+1/2} = \begin{cases} \mathbf{F}_L & S_L \geq 0 \\ \mathbf{F}_L^* = \mathbf{F}_L + S_L (\mathbf{U}_L^* - \mathbf{U}_L) & S_L \leq 0 \leq S^* \\ \mathbf{F}_R^* = \mathbf{F}_R + S_R (\mathbf{U}_R^* - \mathbf{U}_R) & S^* \leq 0 \leq S_R \\ \mathbf{F}_R & S_R \leq 0 \end{cases} \quad (13)$$

where

$$\mathbf{U}_{L,R}^* = \frac{h_{L,R} (S_{L,R} - U_{L,R})}{S_{L,R} - S^*} \begin{bmatrix} 1 \\ S^* \\ C_{L,R} \end{bmatrix} \quad (14)$$

and  $S_{L,R,*}$  can be estimated by the following equations proposed by Fraccarollo and Toro (1995)

$$S_L = \min\{U_L - a_L, U^* - a^*\} \quad (15a)$$

$$S_R = \max\{U_R + a_R, U^* + a^*\} \quad (15b)$$

$$S^* = U^* \quad (15c)$$

where

$$U^* = \frac{1}{2}(U_L + U_R) + a_L - a_R \quad (15d)$$

and

$$a^* = \frac{1}{2}(a_L + a_R) + \frac{1}{4}(U_L - U_R) \quad (15e)$$

The numerical scheme previously described is first-order accurate in space and time. An extension to second-order accuracy is achieved with the TVD version of the second-order accurate weighted average flux (WAF) method given by

$$\mathbf{F}_{i+1/2}^{WAF} = \frac{1}{2}(\mathbf{F}_i + \mathbf{F}_{i+1}) - \frac{1}{2} \sum_{k=1}^N \text{sign}(c_k) \phi_{i+1/2}^k \Delta \mathbf{F}_{i+1/2}^k \quad (16)$$

where  $c_k = S_k \Delta t / \Delta x$  = Courant number associated to the wave speed  $S_k$ ,  $\phi_{i+1/2}^k$  = WAF limiter function and  $\Delta \mathbf{F}_{i+1/2}^k = \mathbf{F}_{i+1/2}^{k+1} - \mathbf{F}_{i+1/2}^k$ .

The source term  $\mathbf{Q}_i^n$  is evaluated using the values at cell center  $i$ . For the calculation of the bed slope term at the cell center  $i$ , the bed elevations at the adjacent cells are used.

The bed evolution is computed from Eq. (4) explicitly

$$z_i^{n+1} = z_i^n + \frac{w_s \Delta t}{2(1-\lambda)} \left[ (c_b - E_s)_i^{n+1} + (c_b - E_s)_i^n \right] \quad (17)$$

where  $z_i$  = cell average bed elevation.

For the application of the numerical model, the flow variables at the boundaries  $x=0$  and  $x=L$  must be known. Boundary conditions were implemented considering two fictitious cells outside the computational domain. The number and type of boundary conditions were defined based on the theory of characteristics (Hirsch, 1990). For a hyperbolic system of equations, the number of specified boundary conditions is the number of characteristics that propagate into the flow domain. The additional required information at the boundaries

was obtained through numerical extrapolation from the interior cells.

The propagation of a turbidity current poses the problem analogous to that of a surge propagation over an initial dry bed. In case of a turbidity current, the initial bed is actually covered with ambient fluid but from a numerical point of view the bed is dry. If a dry bed occurs, then no shock exists and the wave speeds must be estimated by another approach. For the right dry bed case ( $h_L > 0$  and  $h_R = 0$ ) the wave speeds are:

$$S_L = U_L - a_L \quad (18a)$$

$$S_R = U_L + 2a_L \quad (18b)$$

$$S^* = S_R \quad (18c)$$

and for the left dry bed ( $h_R > 0$  and  $h_L = 0$ ) the wave speeds are calculate by

$$S_L = U_R - 2a_R \quad (19a)$$

$$S_R = U_R + a_R \quad (19b)$$

$$S^* = S_L \quad (19c)$$

For the application of the dry bed methodology, the value of the tolerance  $\varepsilon$  must be defined in order to differentiate between dry and wet cells, i.e. a wet cell will be considered when  $h > \varepsilon$ .

Finally, since the numerical scheme is explicit, the time step is restricted by a Courant-Friedrichs Lewy (CFL) type condition

$$\Delta t = Cr \frac{\Delta x}{\max_i \{ |U_i| + \sqrt{gRh_i C_i} \}} \quad (20)$$

where  $Cr =$  Courant number.

## 4 APPLICATIONS OF THE MODEL

In this section the numerical model results are compared with data from laboratory experiments obtained by Alves (2008). Essentially, the experiments were conducted to investigate the characteristics of plunging turbidity currents in reservoirs. Furthermore, depositional records of turbidity currents obtained by Oehy (2003) are used to evaluate the performance of the numerical model.

### 4.1 Description of the laboratory experiments

Alves (2008) conducted a laboratory study of plunging turbidity currents in an experimental facility located at LNEC. The channel is 0.30 m wide, 16.45 m long and 0.75 m deep (maximum).

The channel bottom profile was designed with a special configuration to make it possible to simulate plunging turbidity currents in reservoirs (Fig. 3). The sediment used in the experiments was silica flour with a mean diameter of 20  $\mu\text{m}$  and a density of 2650  $\text{kg/m}^3$ . Velocity profiles were obtained in seven sections by using an Ultrasound Velocity Profiling (UVP) system. Suspended sediment concentration profiles were obtained at two measuring stations by the filtration of siphoned samples collected at different heights above the bed. The results of this laboratory study are also reported in Alves et al. (2008).

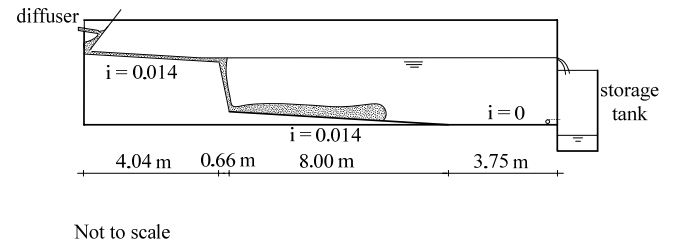


Figure 3. Schematic of the experimental channel (Alves, 2008)

Oehy (2003) performed measurements of the evolution of the sediment layer thickness along the channel due to turbidity currents. The experiments were conducted in a multipurpose flume 0.27 m wide, 8.55 m long and 0.9 m deep. The channel had a bottom slope of 0.0464. The turbidity currents were simulated by the sudden opening of a sluice gate between the mixing tank and the channel. The suspended material used was a fine ground polymer with a density of 1135  $\text{kg/m}^3$  and a mean diameter of 90  $\mu\text{m}$ . Velocity profiles were measured with a UVP device in four sections of the flow. The evolution of the sediment deposits thickness was measured with a special device based on the relation between the electrical resistance of a layer of particles and its thickness (Oehy 2003 and Oehy & Schleiss 2007).

Table 1. Inlet conditions of selected experiments

Author	Exp. No.	$h_0$ (m)	$U_0$ (m/s)	$C_0$ (-)	$B_0 \times 10^{-6}$ ( $\text{m}^3/\text{s}^3$ )
Alves (2008)	S1.15	0.036	0.121	0.00224	158.2
	S1.16	0.036	0.159	0.01250	1158.9
	S1.19	0.036	0.097	0.00644	364.5
	S1.20	0.036	0.148	0.00920	793.4
Oehy (2003)	A04	0.045	0.069	0.02066	85.5
	A06	0.045	0.070	0.02610	109.5
	A07	0.045	0.041	0.03448	84.3

Among the several experiments conducted by Alves (2008) and Oehy (2003), seven were selected for numerical simulation. The initial conditions for selected experiments are given in Table 1. The inlet Richardson number, defined as  $Ri = gRC_0 h_0 / U_0^2$ , was less than unity, i.e., the

generated turbidity currents were supercritical. Also, the Reynolds numbers were high enough to ensure turbulent flows.

For the numerical computations a spatial step  $\Delta x = 0.05$  m and a Courant number  $Cr = 0.98$  are used. The values of other input parameters like the tolerance  $\varepsilon$  for the application of the dry bed methodology, the bed friction coefficient,  $C_D$ , and the relation  $c_b/C$  are listed in Table 2. The experiments used sediments with an almost uniform grain size distribution. The particle fall velocity ( $w_s$ ) was determined by the Stokes law considering the particles mean diameter.

Table 2. Values of the input parameters used in the numerical simulations

Author	Exp. No.	$\Delta x$ (m)	Cr (-)	$\varepsilon$ (m)	$C_D$ (-)	$c_b/C$ (-)
Alves (2008)	S1.15	0.05	0.98	$10^{-3}$	0.02	1.5
	S1.16				0.02	1.8
	S1.19				0.02	1.9
	S1.20				0.02	1.9
Oehy (2003)	A04	0.05	0.98	$5 \times 10^{-3}$	0.01	1.3
	A06				0.01	1.3
	A07				0.015	1.8

#### 4.2 Results of numerical simulations and comparisons with laboratory experiments

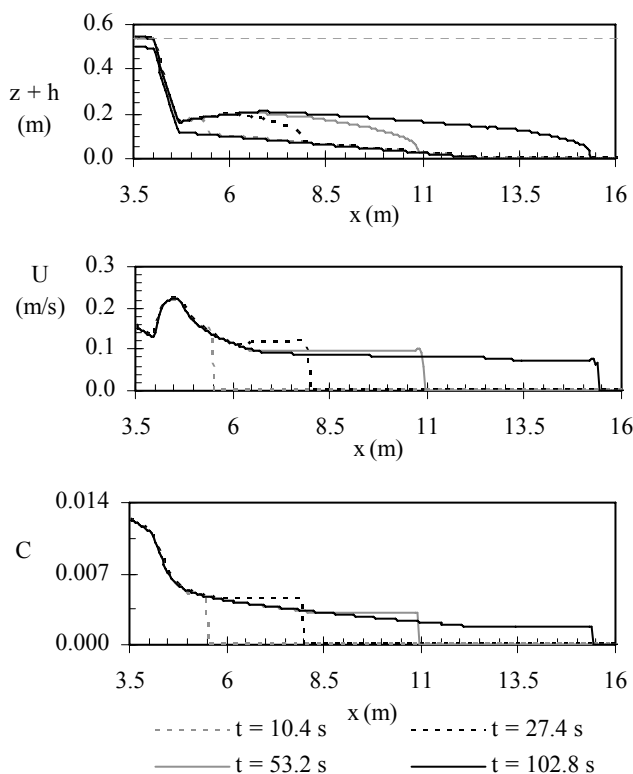


Figure 4. Numerical simulation of a turbidity current propagation along the flume (experiment S1.16)

An example of numerical results obtained for Alves (2008) experiments, showing time-dependent profiles of current height,  $z+h$ , depth-averaged velocity,  $U$ , and depth-averaged suspended sediment concentration,  $C$ , in the longitu-

dinal direction, is given in Fig. 4 for experiment S1.16. During the progression of the turbidity current, a strong decrease of the suspended sediment concentration and an increase of flow thickness occur primarily due to water entrainment along the flume. Furthermore, the currents are also depositing sediments and so they are slowly decelerating.

The front of a turbidity current is characterized by strong gradients in height, velocity and concentration, since these variables are zero downstream. The computational results yields steep fronts without numerical oscillations.

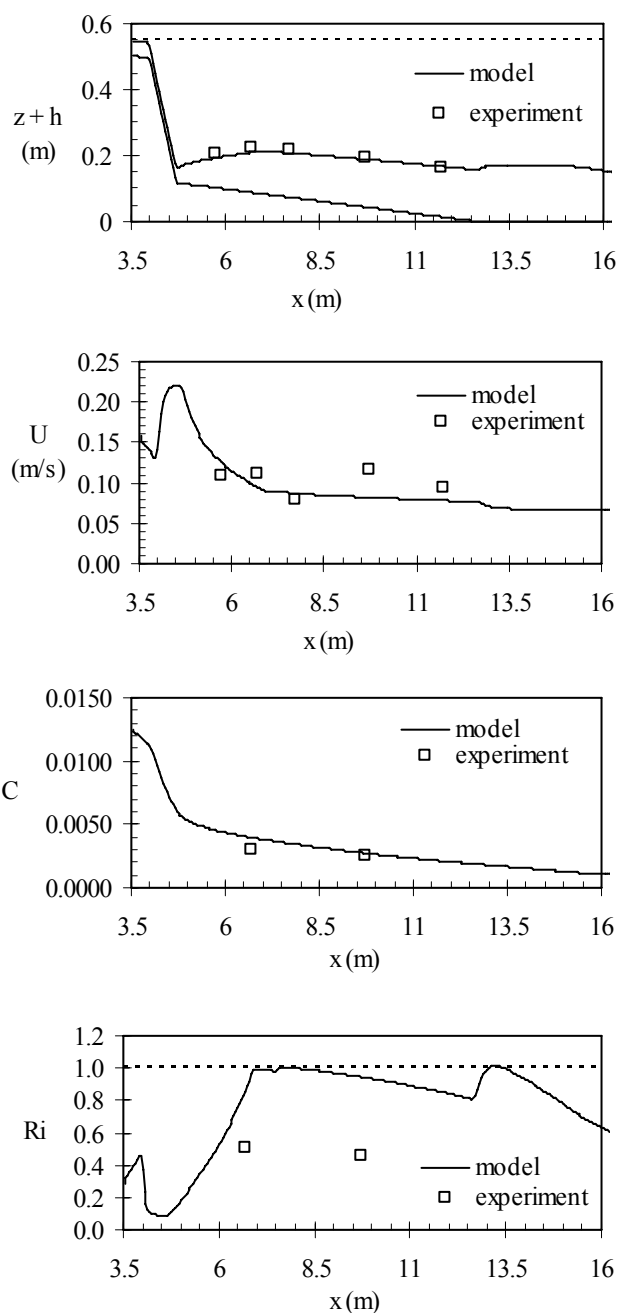


Figure 5. Comparison of numerical results with laboratory measurements (experiment S1.16)

The comparison between the numerical results and the observed values of current thickness,

depth-averaged velocity, suspended sediment concentration and Richardson number are presented in Fig. 5 and Fig. 6 for experiments S1.16 and S1.15, respectively.

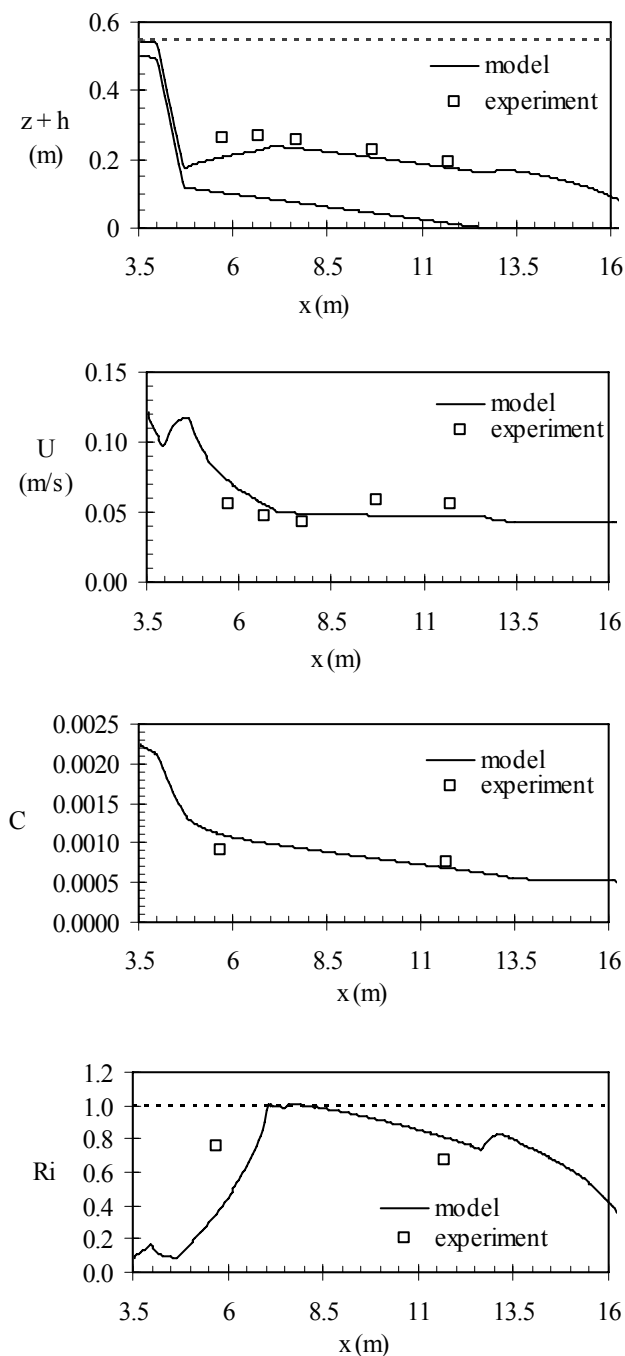


Figure 6. Comparison of numerical results with laboratory measurements (experiment S1.15)

In general, the agreement between computed and observed values is good, except immediately downstream the abrupt slope transition where the model underpredicts the currents thickness and overpredicts its suspended sediment concentration. This is most likely due to the intense mixing process between the underflow and the ambient fluid in the plunging region. In the experiments reported in Alves (2008), the plunging occurs immediately after the slope break due to the sud-

den change in the flow depth. In this region, high values of the mixing coefficient of ambient fluid into the underflow were obtained, which was attributed to the effect of the steepness of the channel bottom on the mixing process.

In the channel slope transition, although an increase of the current thickness was observed no change in the flow regime could be confirmed. For the currents where suspended sediment concentration profiles were measured, the Richardson number,  $Ri$ , remained less than the unity (Fig. 5 and Fig. 6).

Fig. 7 shows a comparison of the predicted and measured front velocities ( $U_f$ ). In the same figure values for Oehy experiments are also included. From this figure it is seen that the model overpredicts the front propagation velocity. This result may be related with the fact that the majority of the laboratory experiments are conducted in relatively shallow waters and not in a deep ambient fluid as assumed in depth-averaged model formulation. Furthermore, the measured velocity profiles exhibit a reverse flow produced by the shear stress at the interface of the turbidity current and the ambient fluid (Oehy 2003 and Alves 2008). This reverse flow may act to increase the interfacial friction thus decreasing the current front velocity observed in the experiments.

A similar tendency to over estimate the current front velocity was observed by other authors that used the layer-averaged formulation but different numerical schemes (Choi & García 1995, Sloff 1997 and Bradford & Katopodes 1999).

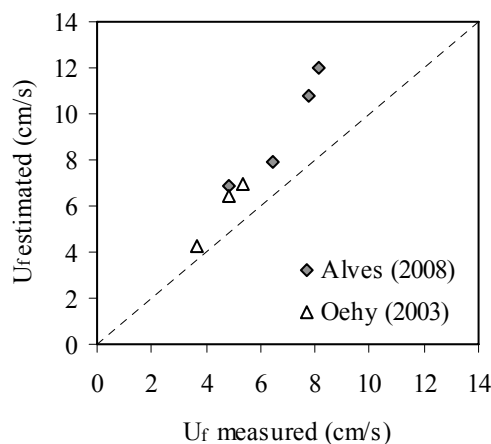


Figure 7. Comparison of numerical results with laboratory measurements (experiment S1.15)

To verify the numerical model ability to predict bed level evolution, a comparison of the numerical and measured bed deposition profiles for three experiments conducted by Oehy (2003) is presented in Fig. 8. As the current moves downstream, the suspended sediment settles out of the turbidity current and deposits along the channel.

The agreement between numerical results and measurements is very good. In case of experiment A07, there is a disagreement between calculations and measurements of the bed levels in the initial part of the channel. These differences seem to be attributable to the influence of the inlet conditions in the laboratory experiments and not to any shortcoming of the numerical scheme. Indeed, as reported by Oehy (2003) and Oehy & Schleiss (2007), near the channel inlet the intense mixing and high velocity of the current tended to make the sedimentation pattern irregular in some experiments. Downstream of this region the bed levels are well reproduced by the numerical model.

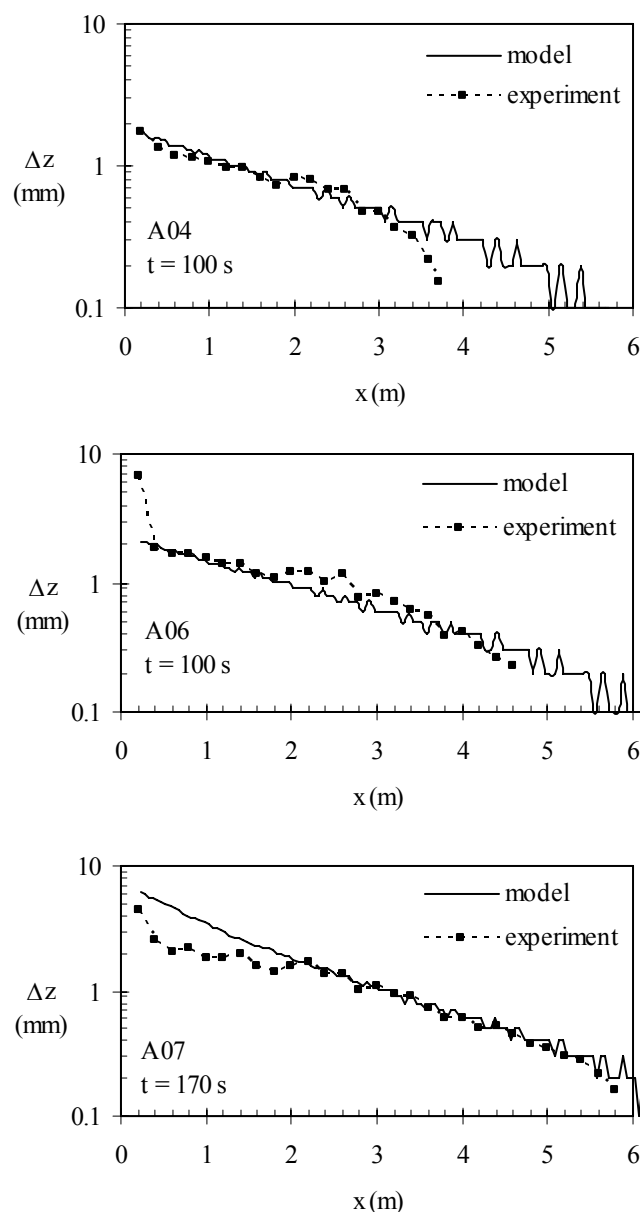


Figure 8. Comparison of computed and measured sediment deposition by turbidity currents along the flume (experiments A04, A06 and A07)

## 5 CONCLUSIONS

A numerical model for one-dimensional turbidity currents driven by uniform sediments is proposed in this paper. The model is based on the layer-averaged formulation which consists of a system of hyperbolic partial differential equations. To solve the governing equations, a finite volume method was adopted. The HLLC Riemann solver has been implemented in the TVD version of the second-order WAF method.

The numerical model has been applied to the simulation of turbidity currents based on the laboratory experiments conducted by Alves (2008) and Oehy (2003). The model is able to simulate the current's hydrodynamics and deposition. The computed profiles of the current thickness, layer-averaged velocity, layer-averaged suspended sediment concentrations and bed deposits show good agreement with the experimental data. The computed velocity of the turbidity current front is generally overestimated which is attributable to the limitations of single layer formulation and to relatively small scale laboratory facilities. Future research will include extensions to two-dimensional flows and the transport of nonuniform sediments.

## ACKNOWLEDGMENTS

The authors acknowledge the financial support of the Portuguese Foundation for Science and Technology under the research project POC-TI/ECM/45778/2002 – “Sedimentation in reservoirs by turbidity currents”.

## REFERENCES

- Alves, E. 2008. Sedimentação em albufeiras por correntes de turbidez (Reservoir sedimentation due to turbidity currents). Dissertação de Doutoramento (PhD Thesis). Universidade Técnica de Lisboa, Instituto Superior Técnico, Lisboa. (in Portuguese)
- Alves, E., González, J., Freire, P., Cardoso, A. H. 2008. Experimental study of plunging turbidity currents in reservoirs. River Flow 2008 – International Conference on Fluvial Hydraulics, Çesme-Izmir, Turquia, 3-5 September, 1157-1164.
- Bradford, S., Katopodes, N., Parker, G. 1997. Characteristic analysis of turbid underflows. *Journal of Hydraulic Engineering*, 123(5), 420-431.
- Bradford, S., Katopodes, N. 1999. Hydrodynamics of turbid underflows. I: Formulation and numerical analysis. *Journal of Hydraulic Engineering*, 125(10), 1006-1015.
- Cao, Z., Pender, G., Wallis, S., Carling, P. 2004. Computational dam-break hydraulics over erodible sediment bed. *Journal of Hydraulic Engineering*, 130(7), 689-703.
- Choi, S.-U., García, M. H. 1995. Modeling of one-dimensional turbidity currents with a dissipative-



- Galerkin finite element method. *Journal of Hydraulic Research*, 33(5), 623-648.
- Choi, S.-U., 1998. Layer-averaged modeling of two-dimensional turbidity currents with a dissipative-Galerkin finite element method. Part I: Formulation and application example. *Journal of Hydraulic Research*, 36(3), 339-362.
- Fan, J., Morris, G. L. 1992. Reservoir sedimentation. I: Delta and density current deposits. *Journal of Hydraulic Engineering*, 118(3), 354-369.
- Fraccarollo, L., Toro, E. F. 1995. Experimental and numerical assessment of the shallow water model for two-dimensional dam-break type problems, *Journal of Hydraulic Research*, 33(6), 843-864.
- Fraccarollo, L., Capart, H., Zech, Y. 2003. A Godunov method for the computation of erosional shallow water transients. *International Journal for Numerical Methods in Fluids*, 41, 951-976, DOI: 10.1002/flid.475.
- Hirsch, C. 1990. Numerical computation of internal and external flows. Volume 2 – Computational methods for inviscid and viscous flows. John Wiley & Sons.
- ICOLD (1999). Dealing with reservoir sedimentation. Guidelines and case studies. Bulletin 115, International Commission on Large Dams.
- Kostic, S., Paker, G. 2003. Progradational sand-mud deltas in lakes and reservoirs. Part 1. Theory and numerical modelling. *Journal of Hydraulic Research*, 41(2), 127-140.
- Kostic, S., Paker, G. 2006. The response of turbidity currents to a canyon-fan transition: internal hydraulic jumps and depositional signatures *Journal of Hydraulic Research*, 44(5), 631-653.
- Oehy, C. 2003. Effects of obstacles and jets on reservoir sedimentation due to turbidity currents. Thèse de doctorat N° 2684, Ecole Polytechnique Fédérale de Lausanne.
- Oehy, C., Schleiss, A. 2007. Control of turbidity currents in reservoirs by solid and permeable obstacles. *Journal of Hydraulic Engineering*, 133(6), 637-648.
- Parker, G., Fukushima, Y., Pantin, H. M. 1986. Self-accelerating turbidity currents, *Journal of Fluid Mechanics*, 171, 145-181.
- Parker, G., García, M. H., Fukushima, Y., Yu, W. 1987. Experiments on turbidity currents over an erodible bed, *Journal of Hydraulic Research*, Vol. 25, 123-147.
- Sloff, C. J. 1997. Sedimentation in reservoirs. Communications on Hydraulic and Geotechnical Engineering, Report No. 97-12, Delft University of Technology, The Netherlands.
- Toro, E. F., Spruce, M., and Spears, W. 1994. Restoration of the contact surface in the HLL-Riemann solver, *Shock Waves*, 4(1), 25-34.
- Toro, E. F. 1999. Riemann solvers and numerical methods for fluid dynamics. A practical introduction. Springer-Verlag.